IEEE Access
Multidisciplinary ⋮ Rapid Review ⋮ Open Access Journal

Received 15 May 2022, accepted 2 June 2022, date of publication 14 June 2022, date of current version 25 July 2022.

Digital Object Identifier 10.1109/ACCESS.2022.3183094

Positioning for Search and Rescue in GPS-Denied Area by Distributed WiFi RSS-Based DoA Modules

SHIH-YI HUANG AND RUEY-BEEI WU, (Fellow, IEEE)
Department of Electrical Engineering, National Taiwan University, Da'an District, Taipei City 10617, Taiwan
Corresponding author: Shih-Yi Huang (r07942135@ntu.edu.tw)

This work was supported in part by the Ministry of Science and Technology, Taiwan, under Grant MOST 110-2221-E-002-172; and in part by the Higher Education Sprout Project by the Ministry of Education (MOE) in Taiwan under Grant NTU-CC-111L894501.

ABSTRACT Environmental factors affect the Received Signal Strength (RSS) so the received data exhibit random propagation characteristics, such as fading and shadowing effects. This study proposes a Direction of Arrival (DoA) module for the Search and Rescue (SaR) or anti-drone applications, which uses patch antennas and a rat-race coupler as the receivers. An angular estimation is presented for WiFi positioning, using optimally placed DoA antennas and a pseudo-inverse algorithm. The experiment is performed in a university campus with the device under test (DUT) as the transmitter. Using four DoA antennas as receivers at the corners of a 100m×100m region, the mean positioning deviation is about 2m, which is 2% of the region. The confidence range for the estimated positions is also calculated.

INDEX TERMS Optimal DoA placement, rat-race coupler, search and rescue, Wi-Fi positioning.

I. INTRODUCTION

There is an increasing need for positioning using the internet and GPS systems. However, GPS is sometimes blocked by shades, rooftops, ground objects, and is affected by interference in the ionosphere so some studies involve the denial of GPS service or loss of accuracy. Local positioning becomes one of the most exciting features of the next generation of wireless systems. Numerous applications include self-organizing sensor networks, ubiquitous computing, location sensitive billing, context dependent information services, tracking and guiding, search and rescue (SaR), etc. [1].

Typical mountain SaR operations require the localization of the persons involved in accidents in harsh environments. The climber location information systems have been setup in case of distress accidents at the mountainous area, which involves VHF radio wave stations in mountain lodges [2], [3] or drones with WiFi beacons receiver [4]. Location awareness rescue system (LARS) for monitoring rescuers is deployed for informing the mission coordinator in mountain rescue teams via GPRS or WiFi connectivity [5] and even CNN is employed to facilitate SaR from the images taken from drones [6]. All the above methods rely on the operation of GPS for the location transmission.

However, the environment might prohibit the detection of GPS considering the searched people are often sheltered by vegetation, hidden behind a stone, or merged with the ground and in unusual positions due to falls, injuries, or exhaustion. In GPS-denied area where the signals transmit in NLOS and multipath, it is still helpful to locate the position of the last reflection in the multipath, which is near the climbers. The localization is obtained based on path-loss (PL) measurement by the Long-Range (LoRa) technology, but it requires a relatively large number of available PL measurement and the accuracy is low [7].

This study proposes an efficient remedy using the WiFi for which most mountain climbers carry and the operating frequency is higher to allow for better accuracy. The drone can hover above the harsh environment, receiving WiFi signal from the mountaineers and determining the location by the direction of arrival (DoA) instead of PL measurement which is susceptible to the variation of radio propagation in harsh environment.

Other scenarios involve alien or hostile moving targets which may not transmit their GPS locations, making the detection of drones difficult. Currently, communication between the control terminal and the drone or the

The associate editor coordinating the review of this manuscript and approving it for publication was Kegen Yu.

transmission of high-definition images uses the 2.4GHz band signal. Rogue drones have caused a serious threat to the normal operation at civil airports [8]. Airports have been closed due to unidentified drones [9]. It is very difficult to detect small drones in large space so it can take days to resolve the problem, which results in losses and inconvenience for passengers and airlines. Active radar cannot be used to identify drones because their radar cross section is too small. High degree of electromagnetic radiation in urban areas raises the concern of residents so when drones become more ubiquitous, some urban or restricted areas will become no-fly zones [8]. Small and passive radars [10]–[12] that do not transmit signals will then become necessary [13].

Accurate positioning using WiFi has been demonstrated [14]. The received signal strength (RSS) metric is used for fingerprinting-based RADAR algorithm [15], with meters accuracy. Centimetre accuracy is possible using CFR (Channel Frequency Response) for multi-frequency channels [16] or for multiple antennas [17]. However, specific hardware and software requires exhaustive data acquisition and a lengthy training phase for the classification algorithm so this is only suited to indoor environment.

A hybrid analog-digital architecture using pairs of tilted directive antennas was proposed to calculate the DoA of WiFi signals using a digital monopulse function [18]. The DoA is determined by comparing the difference between the RSS at pairs of titled directive antennas. This is suitable for outdoor applications and no expensive hardware is required to process IQ data. It is validated with anechoic chamber measurement, but susceptible to fading and other environmental effects. The architecture is large and the FoV (Field of View) in which the direction can be accurately measured is limited to $\pm 20^{o}$ and the angle error is large at 5^{o}.

Collaborative sensors are used to measure the DoA and RSS and non-cooperative transmitter localization is used, for which the asymptotic performance is theoretically evaluated [19]. In real applications, the method is used to observe the ecological behaviours of bats, using lightweight RF tags. The ratio of the received sum-difference power is used to determine the position [20]. Simulation by maximum likelihood estimation gives an optimal angle error of 5^{o} near the center and 15^{o} near the boundary [21]. The performance of different estimators has been compared [22]. The idea is extended in this study with the following advantageous features:

1) The proposed system uses antennas array but does not need network analyzers for complex phase measurement of receiving signal. By using rat race coupler, users only need to measure the RSS and the sum and difference values are obtained from the commercial off-the-shelve (COTS) WiFi endpoint devices.
2) It can operate in the harsh environments with denial of GPS service where the wave propagation suffers from fading or shadowing effects. Localization of the searched targets does not rely on the path-loss model and the positions of multiple signal sources can be determined through the MAC addresses of the WiFi devices.
3) It can be combined with the drone to have a dynamic and comprehensive search over a large region. The drone hovering in the sky with available GPS can provide DoA's of the searched target from different locations so accurate positioning can be achieved by a single drone.

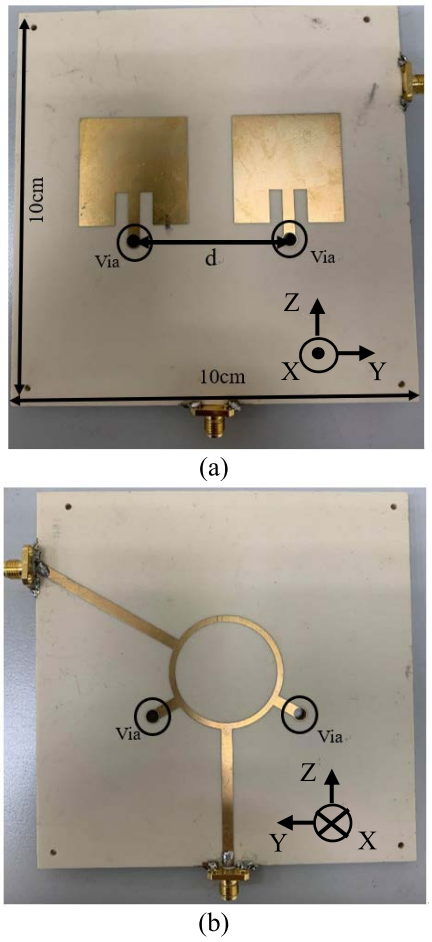

FIGURE 1. DoA module. (a) top view showing patch antennas and (b) back view showing a rat race coupler.

The remainder of this study is organized as follows. Section II presents the design of a small and planar DoA receiver module that uses two patch antennas and a rat race coupler. The RSS ratio between the difference and sum ports is measured in the open space and verified using simulation and anechoic chamber measurement in Section III. Section IV calculates the optimal DoA using the measured data. The positioning algorithm from distributed DoA modules and the confidence range of prediction is detailed in Section V. Conclusions and discussion are drawn in Section VI.

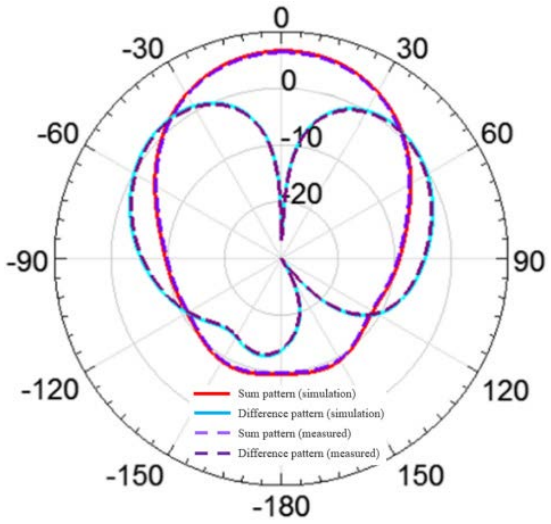

FIGURE 2. Simulated and measured patterns in X-Y plane, at the sum and difference ports, which are respectively shown as solid and dashed curves.

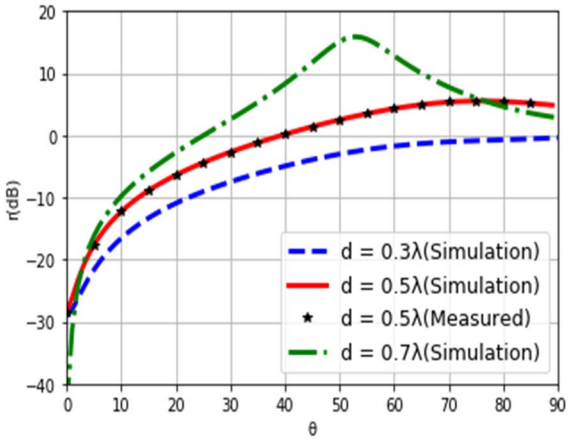

FIGURE 3. Voltage ratio between the difference and sum ports of the DoA versus incoming signal angle, in terms of antenna separation.

II. DOA MODULE WITH PATCH ANTENNA AND A RAT RACE COUPLER

Without loss of generality, the study employs channel 6 of the WiFi 2.4 GHz band, for which the frequency range is centered at 2.437GHz with bandwidth of 22 MHz. The proposed DoA module uses a three-layer PCB for which the top metallurgy is two patch antennas, the middle is a papery ground plane, and the bottom is a rat race coupler [23] as shown in Fig, 1. The circuits are connected by vias that pass through the middle ground plane. The PCB uses ROGERS 4003C with a layer thickness of 1.524 cm, dielectric constant of 3.55, and loss tangent of 0.0027.

The direction of incoming signal is determined using the ratio of the RSS at the difference and sum ports (Fig. 1(b)) of the rat race coupler. Fig. 2 shows the simulated patterns for the two ports, which are also measured in an Anechoic Chamber. The simulated and measured patterns are represented by solid and dashed curves, respectively, and the unit is in dB. The results for both are in good agreement. Most of the power is due to forward radiation. Back radiation is 16dB less. Therefore, the DoA uses the incoming signal from the forward radiation and back radiation has no significant effect.

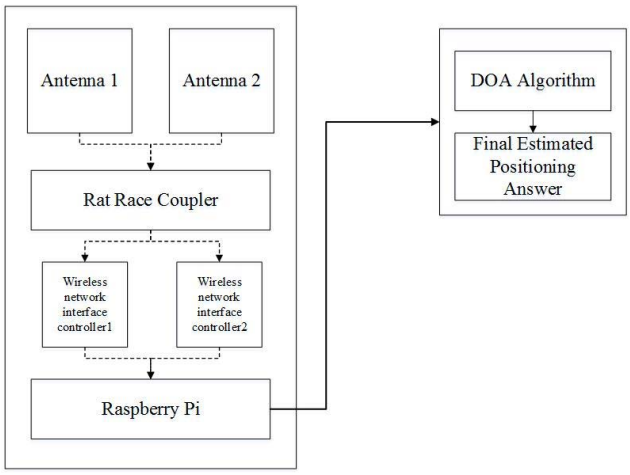

FIGURE 4. Block diagram of the DoA module at receiving end.

The RSS ratio r is defined as the ratio of the RSS between the difference and sum ports. It is usually expressed in terms of dB and can thus be determined by subtracting difference pattern from sum pattern. Based on the simulated patterns, the RSS ratio r versus the incoming signal angle θ is plotted in Fig. 3. The separation between patch antennas is chosen as a parameter, i.e., $d = 0.3, 0.5$, and 0.7λ. The FoV can be easily recognized from r. For smaller antenna separation, the FoV increases, but the accuracy with which the angle is measured decreases.

This study uses an antennas separation $d = \lambda/2$ to achieve the best FoV and accuracy. The FoV is approximately 50^{o}. Only the signal strength is measured by the DoA module. Therefore, two angles - θ and -θ - correspond to the same value of r, so a mechanism to discriminate the ambiguity is necessary.

The Friis formula states that the RSS attenuates as the distance between the signal source and the DoA module increases. Nonetheless, the relationship $r = g(\theta)$ is theoretically independent of the distance. This is validated experimentally in the anechoic chamber with perfect agreement between the simulation and measured data, as shown by the dots in Fig. 3. The DoA module only measures the incoming angle and not the distance so two or more DoA modules are necessary to allow accurate detection of the position of an unknown signal source.

The block diagram of the DoA module at the receiving end is shown in Fig. 4. The received signals at the patch antennas 1 and 2 are combined in the rat race coupler and are respectively measured at the difference and sum ports.

The RSS at the difference and sum ports is retrieved by the wireless network interface controllers (NIC) and is input into the connection slot for a Raspberry Pi (RPi 3B$^+$) via a USB - Type A connector and a SMA extension cable. During the receiving process, the data is stored in the hard disk of RPI 3B+, and a program that is detailed later in this paper processes this data when measurements are complete.

FIGURE 5. Measurement setup at NTU campus, where Tx is WiFi AP and Rx is DoA module mounted on a turn table and located 30 or 40 meters in front of WiFi AP.

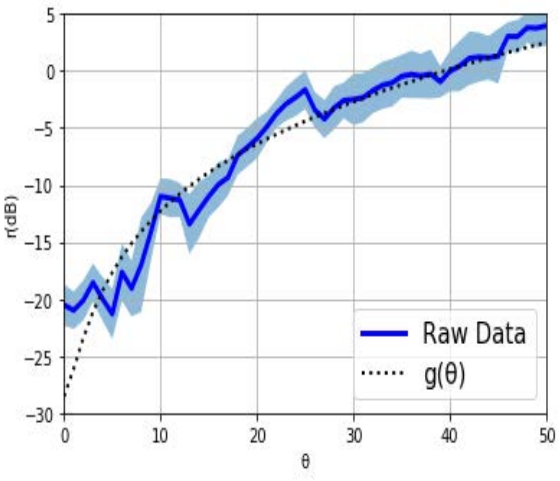

FIGURE 6. Distribution of measured raw data.

III. EXPERIMENTAL CHARACTERIZATION OF WIFI AP's

The capability of the DoA module to determine the signal angle is characterized using WiFi AP's, which are subject to various unexpected interference sources and random noises. The test field for this study is the open playground in the university campus, as shown in Fig. 5. Tx and Rx are one-meter above the ground. Tx transmits a 2.4GHz Wi-Fi signal. Rx is 30 or 40 meters in front of Tx to determine how r is related to θ at different distances. At each distance, the measurement is repeated 40 times for each angle, which is set by the turn table from 0 to 50^o at one-degree increment.

The raw measurement data for distances of 30 and 40 meters is shown in Fig. 6. The blue solid line is the mean, the light blue color denotes plus and minus one standard deviation σ_r, and the black dashed line is the value of g(θ) that is measured in the anechoic chamber. The outliers outside $3\sigma_r$ are ignored.

The raw data depends on g(θ), but is subject to variations due to the effect of the environment on the radio waves. This plot also shows that the mean for the raw data is biased and the variations depend on the angle. The deviation for small angles is relatively large so the statistical characteristics of the measured data are related to the angle.

For example, when $r < -20$ dB, the measured angles are distributed at small angles, and their distribution is more concentrated. The reason is that g(θ) has a large slope when the angle is small, and the change of θ relative to r is less sensitive than when $r > 2$ dB. As a result, when the angle θ received by the rat race coupler is small, the measured r has larger relative error but the angle error determined by r is smaller.

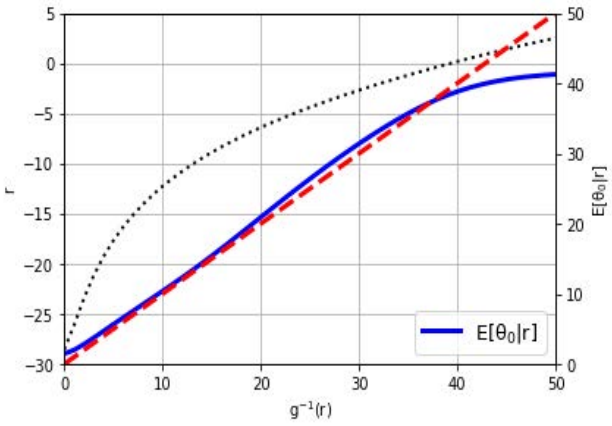

FIGURE 7. Relationship between r, $g^{-1}(r)$, and $E[\theta_0|r]$.

IV. DOA CALCULATION FROM MEASURED DATA

It is desired to calculate the direction of the incoming signal source. The conditional probability $p(r|\theta)$ of the RSS ratio r is calculated using all of the received data in Fig. 6 for the source angle θ. Let θ_0 denote the estimated angle given the measured r. The conditional probability $p(\theta_0|r)$ can be calculated by

$$p(\theta_0|r) = \frac{p(r|\theta_0)\, p(\theta_0)}{p(r)} \tag{1}$$

where $p(\theta)$ is assumed to be uniform between $\theta = 0^o$ to 50^o and $p(r) = \int p(r|\theta)\, p(\theta)\, d\theta$. Then, the estimated angle versus the measured r is given by the Bayesian

prediction [24], [25], *i.e.*,

$$\hat{\theta}\,(r) = \mathrm{E}[\theta_0|r] \tag{2}$$

Fig. 7 shows the relation between measured r, the true angle from anechoic chamber $\theta = \mathrm{g}^{-1}\,(r)$, and the estimation $\hat{\theta}\,(r)$ under the interference in the real measurement scenario. This is a biased estimation as noted from the discrepancy between the dashed and solid curves. The angle determination error is larger for large θ. Over the most angle range $0 < \theta < 40^{\mathrm{o}}$, the error is smaller than 2^{o} and the angle has taken into account the wave propagation effects for RSS of received Wi-Fi signal in the real environment

In the simulation for positioning, the measured value for r at a specific angle θ is a random variable and for each, the prediction gives an estimated angle θ_0. A change in the value of r affects θ_0. For σ_{θ_0}, the mse (Mean Squares Error) is calculated to determine the variance for the estimated angle:

$$\mathrm{mse}_r(\hat{\theta}) = \int_{\theta} \mathrm{p}\,(\theta_0 \,|\, \mathrm{r})(\mathrm{E}[\theta_0|\mathrm{r}] - \theta))^2 \mathrm{d}\theta_0 \tag{3}$$

where $r = g(\theta)$.

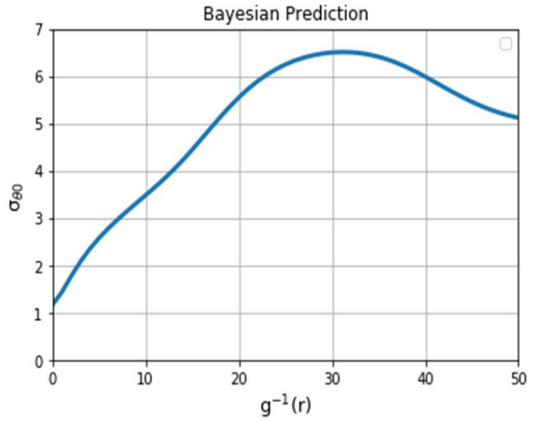

FIGURE 8. Standard deviation of estimated angle, σ_{θ_0}, versus ground truth angle $\sigma = g^{-1}\,(r)$.

Using (3) and the square root to obtain σ_{θ_0}, Fig. 8 shows the change in the estimated angular error versus the ground truth angle θ. The angular error is small when θ is small, even if the value for σ_r is the largest, because g(θ) has a large gradient. At a larger angle, σ_r is smaller, the calculated angular error increases since the gradient of g(θ) is smaller.

The results show that $\sigma_{\theta_0}$is smaller and the angular accuracy is better for small θ. To increase the accuracy of the estimated angle, the antenna directivity may be increased, but the range of the span is then decreased as described in Section II. The relationship of mean and standard deviation versus the angle θ in Figs. 7 and 8, respectively, means that the positioning accuracy can be calculated by simulation.

V. POSITIONING ALGORITHM

The positioning algorithm to determine the position (x, y) of the device under test (DUT) can be briefly described here, and details will be explained by a following example.

Consider a region in which the DUT transmits the signal and there are N receivers in the exterior with locations known in prior. Each DoA module in the receiver can determine the incident angle to the broadside direction of the module antennas. A linear equation governing the unknown DUT position (x, y) can be constructed. Multiple receivers construct multiple equations and then the desired (x, y) can be obtained from the solution of a system of equations,

Since the measurement in the present method is phase-less, there might be $\pm\theta$ two possible angles and the associated two governing equations for each reviver. As a result, there may be at most 2^N possible solutions for the DUT position (x, y). A method of minimal residual sum is proposed to select the most probable solution.

A. MORE ACCURATE SOLUTION USING PSEUDO INVERSE

To facilitate the analysis, this study uses a square of 100 m × 100 m, with DoA modules at the four corners ($N = 4$). The accuracy of the solution depends on the orientation of the four modules. Case 1 uses four DoA modules with the $\theta = 0$ axis aligned with the x axis, and Case 2 has the $\theta = 0$ axis pointing to the center of the square region.

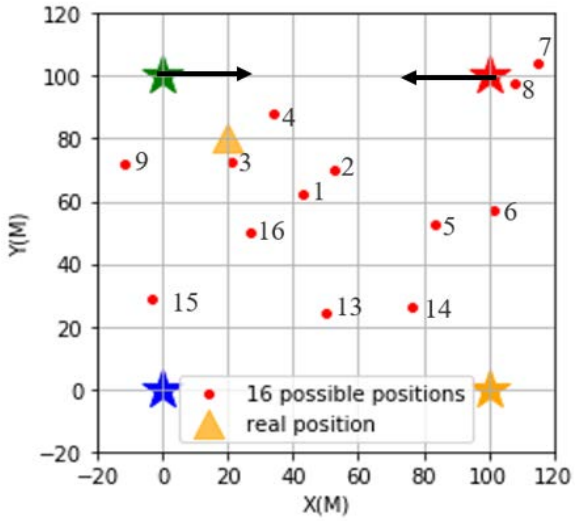

FIGURE 9. Distribution of 16 possible solution points for positioning.

The four DoA modules are located at $\{(c_{xi}, c_{yi})\,|i = 1, .., 4\} = \{(0, 0), (100, 0), (0, 100), (100, 100)\}$. The scenario for Case 1 is shown in Fig. 9, where modules 1 and 3 face to $+x$ direction and modules 2 and 4 to -x direction. For the i-th DoA module ($i = 1,\ldots, 4$), if the true position of the source is (x, y), the true angle $\theta_{\mathrm{i}} = \tan^{-1}\left|\frac{\mathrm{y}-\mathrm{c_{yi}}}{\mathrm{x}-\mathrm{c_{xi}}}\right|$ is calculated. The estimated angle is calculated using the value of mean $\hat{\theta}_i$ from Fig. 7 and the standard deviation from Fig. 8. The position of the source must satisfy the linear equations

$$\sin\hat{\theta}_i \cdot x \pm \cos\hat{\theta}_i \cdot y = b_i = \sin\hat{\theta}_i \cdot c_{xi} \pm \cos\hat{\theta}_i \cdot c_{yi} \quad \text{for } i = 1, .., 4 \tag{4}$$

where $\hat{\theta}_i$ denotes the angle with respect to the $+x$ axis. Given the positions of the four DoA modules, the unknown position (x, y) satisfies 4 linear equations in (4) and is solved by pseudo inverse method.

In more details, the four equations in (4) can be written as a matrix equation $\mathbf{Hx} = \mathbf{b}$, where the vector $\mathbf{x} = [x, y]^{\mathrm{T}}$ and

$$\mathrm{H} = \begin{bmatrix} \sin\hat{\theta}_1 & -\cos\hat{\theta}_1 \\ \sin\hat{\theta}_2 & \cos\hat{\theta}_2 \\ \sin\hat{\theta}_3 & \cos\hat{\theta}_3 \\ \sin\hat{\theta}_4 & -\cos\hat{\theta}_4 \end{bmatrix}, \mathrm{b} = \begin{bmatrix} b_1 \\ b_2 \\ b_3 \\ b_4 \end{bmatrix} \tag{5}$$

The pseudo inverse solution can be given by $\mathbf{x} = (\mathbf{H}^{\mathrm{T}}\mathbf{H})^{-1}\mathbf{H}^{\mathrm{T}}\mathbf{b}$.

B. SELECTION OF SOLUTION BY MINIMUM RESIDUAL SUM

The ratio r for the DoA module is symmetric with respect to $\theta = 0$, so θ and -θ cannot be distinguished unless the RSS and the phases are measured. Each equation in (4) corresponds to two equations. Combining all $2^N = 16$ possibilities gives 16 solution points.

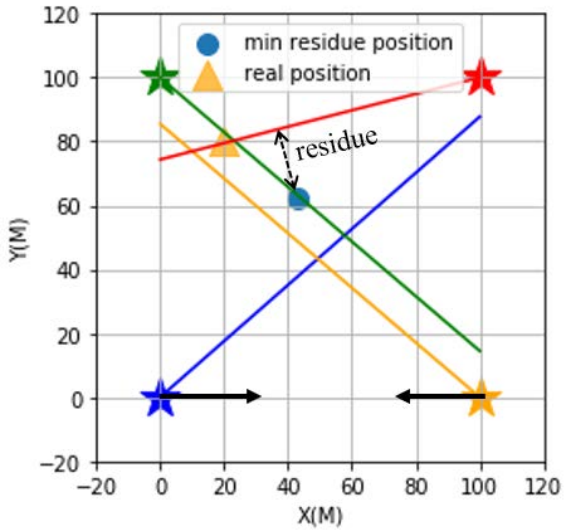

FIGURE 10. Calculation of the residue sum for a possible solution point.

To select the most suitable point, the residue of the solution point is defined as the separation from the related line in the space. Fig. 10 shows the four lines that correspond to the point 1 in Fig. 9 and the residue for one line. Summing the 4 residues gives the residual sum as listed in Table 1. The point with the minimum residual sum is selected as the solution. The criterion does not guarantee the solution closest to DUT, but excludes those that are unlikely to be correct.

Fig. 9 shows that if the ground truth for the DUT is (20, 80), the small solid dots are 16 possible locations for the source. Some of these are out of range and are not shown here. Point 1 (the large solid circle in Fig. 10) has the smallest residual sum. This is close to the true point (20, 80) in Fig. 9, but is probably not the closest.

TABLE 1. Residue values of 16 points. (Unit:m).

#1	#2	#3	#4	#5	#6	#7	#8
31	51	54	65	70	72	100	100
#9	#10	#11	#12	#13	#14	#15	#16
58	56	46	66	98	110	114	134

If the DUT is symmetric to the four DoA modules, two solutions can have the same value of minimum residual sum. This symmetry is eliminated if the DUT is slightly moved. This is usually the case in reality because the DUT moves and there is no ambiguity in determining the best solution point.

The FoV also affects the solution accuracy. The FoV for this study is about 50^{o} and the solution point 1 is near the boundary of FoV for DoA modules 1 and 2, where the angular accuracy is decreased, so solution point 1 still exhibits significant deviation from the ground truth. A better option is to orient the DoA modules to face to the center of the region. This is discussed later.

C. EFFECTS OF DOA MODULE ORIENTATION

The orientation of DoA modules significantly affects the positioning accuracy. To determine the effects of orientation, DoA modules in the same location but with different orientations are used. A contour map is constructed to characterize the positioning performance.

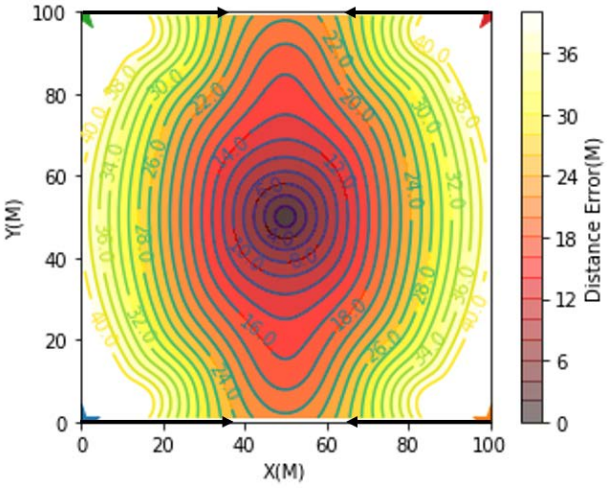

FIGURE 11. Contour map of positioning error for Case 1 using four DoA modules facing in the +x and −x directions.

Fig. 11 shows the contour map for the deviation from the correct position of DUT. The DUT is varied from (1, 1) to (99, 99) with increment of 1 meter and the estimated positions are obtained using the proposed algorithm. The most accurate positioning is at the center of the region, with a deviation of less than 2 meters. The deviation increases quickly as the

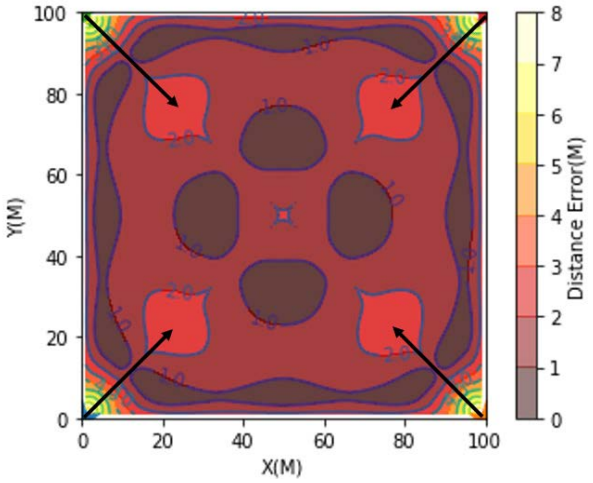

FIGURE 12. Contour map of positioning error for Case 2 using four DoA modules facing the center.

DUT moves away from the center and has a value of more than 40 meters near the boundary of the square space.

Case 2 uses four DoA modules pointing to the center of the region, so the modules at (100, 0) and (0, 100) are rotated clockwise through 45° and the modules at (0, 0) and (100, 100) are rotated counter-clockwise through 45°. The same procedure is used to calculate the DUT positions. Fig. 12 shows the contour map for the positioning error.

It is found that except for the points near the four DoA modules, the positioning error for the entire region inside the 100 m × 100 m is less than 3 m. The orientation is such that the DUT is near small angle of θ with respect to at least two DoA modules. The accuracy is almost 10 times greater than that for Fig. 11. The best accuracy is obtained if all DoA modules face the center of the region.

D. CONFIDENCE RANGE USING A PSEUDO MONTE CARLO METHOD

The positioning error denotes the difference between the average estimated position and the ground truth. However, the estimated position (X, Y) is random and has a probability distribution. If the true position of DUT is (x_0, y_0), the confidence range must be calculated.

For the simulation, the true angle θ can be calculated for a specific DUT position. The measured ratio r is also a random variable, so the standard deviation σ_{θ_0} for the estimated angle can be obtained using Fig. 8. The final predicted positions have a range of changes. A Monte Carlo simulation is used to calculate the confidence interval for the prediction, but this involves an extremely large computation. A pseudo Monte Carlo simulation is faster and gives an estimate of the confidence range.

The entire solution process is analytical and has its continuity. There are four DoA modules so the solution process involves four estimated angles $\hat{\theta}(r) = E[\theta_0|r]$. For the simulation, the angle has three values: $\hat{\theta}$, $\hat{\theta}+\sigma_{\theta_0}$, and $\hat{\theta}-\sigma_{\theta_0}$ to reasonably cover the sample space for the angle. Therefore, $3^4 = 81$ points are used for the simulation and 81 estimated points $\{(x_j, y_j)|j = 1, \ldots, 81\}$ are calculated.

The estimated point (X, Y) is a random variable. If the changes in the distribution of X and Y axes are $\sigma_{\tilde{x}}$ and $\sigma_{\tilde{y}}$, respectively, and $\sigma_{\tilde{x}\tilde{y}}$ is the correlation, then to calculate the confidence range, the major and minor axes of the ellipse enclosing the 81 estimated points mush be calculated. The ellipse center is

$$x_c = \frac{1}{M}\sum_{j=1}^{M}\tilde{x}_j, \quad y_c = \frac{1}{M}\sum_{j=1}^{M}\tilde{y}_j \tag{6}$$

where M = 81. Then, $\sigma_{\tilde{x}}$, $\sigma_{\tilde{y}}$ and $\sigma_{\tilde{x}\tilde{y}}$ satisfy

$$\begin{bmatrix} \sigma_{\tilde{x}}^2 & \sigma_{\tilde{x}\tilde{y}} \\ \sigma_{\tilde{x}\tilde{y}} & \sigma_{\tilde{y}}^2 \end{bmatrix} = \frac{1}{\mathrm{M}} \begin{bmatrix} (\tilde{x}_1 - \mathrm{x_c}), \cdots, (\tilde{x}_\mathrm{M} - \mathrm{x_c}) \\ (\tilde{y}_1 - \mathrm{y_c}), \cdots, (\tilde{y}_\mathrm{M} - \mathrm{y_c}) \end{bmatrix}_{2\mathrm{xM}} \cdot \begin{bmatrix} (\tilde{x}_1 - \mathrm{x_c}), & (\tilde{y}_1 - \mathrm{y_c}) \\ \vdots & \vdots \\ (\tilde{x}_\mathrm{M} - \mathrm{x_c}), & (\tilde{y}_\mathrm{M} - \mathrm{y_c}) \end{bmatrix}_{\mathrm{Mx2}} \tag{7}$$

If the long and short axes of the ellipse are b and a, respectively, (7) can be related to the two axes in the form

$$\begin{bmatrix} \sigma_{\tilde{x}}^2 & \sigma_{\tilde{x}\tilde{y}} \\ \sigma_{\tilde{x}\tilde{y}} & \sigma_{\tilde{y}}^2 \end{bmatrix} = A \cdot \begin{bmatrix} (\mathrm{a}\cos\varphi)^2 + (\mathrm{b}\sin\varphi)^2, & (\mathrm{a}^2 - \mathrm{b}^2)\sin\varphi\cos\varphi \\ (\mathrm{a}^2 - \mathrm{b}^2)\sin\varphi\cos\varphi, & (\mathrm{a}\sin\varphi)^2 + (\mathrm{b}\cos\varphi)^2 \end{bmatrix} \tag{8}$$

where A is a certain proportional constant and ϕ is the slant angle of the ellipse. The constant A can be eliminated by solving (8), and it is not difficult to obtain

$$\varphi = \frac{1}{2}\tan^{-1}\left(\frac{2\sigma_{\tilde{x}\tilde{y}}}{\sigma_{\tilde{x}}^2 - \sigma_{\tilde{y}}^2}\right), \tag{9}$$

and the axes ratio

$$\frac{a^2}{b^2} = \frac{(\sigma_{\tilde{x}}\cos\varphi)^2 - (\sigma_{\tilde{y}}\sin 2\varphi)^2}{(\sigma_{\tilde{y}}\cos\varphi)^2 - (\sigma_{\tilde{x}}\sin 2\varphi)^2} \tag{10}$$

The ellipse is calculated using the 81 points and the axes ratio (10), and it is formed by the angles in (9) over their corresponding mean $\pm\sigma_{\theta_0}$. If the values of σ_{θ_0} are similar, the ellipse corresponds to a circle in the angular domain with radius $\sqrt{2}\sigma_{\theta_0}$. Integrating the probability density function for a normal distribution over the circle gives a confidence level of $1 - e^{-1} = 63\%$. A pseudo inverse is used so the actual confidence level is greater.

For Case 2, the ellipses in Fig. 13 show the confidence range of the estimated positions using the pseudo Monte Carlo method. The ellipse at the center is a circle and its area is the smallest. This is expected from Fig. 8 and the smaller the angle deviation σ_{θ_0}, the greater is the positioning accuracy. The ellipse is significantly slanted for DUT close to the periphery. The area of the range is greater and the error is larger.

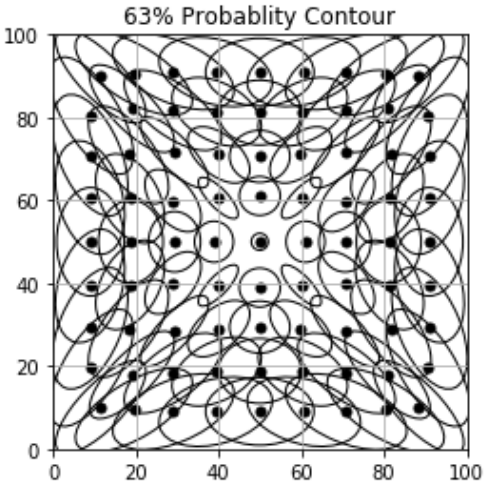

FIGURE 13. Range of estimated positions with an approximate confidence level of 63%.

VI. CONCLUSION AND DISCUSSION

This study employs DoA modules for positioning using the RSS for Wi-Fi at 2.4GHz. The DoA module uses two patch antennas in one side of the PCB and a rat race coupler in the other side. The outputs for the patch antennas are connected to the input ports of the rat race coupler through vias to give sum and difference ports. The separation between two patch antennas is $\lambda/2$ to achieve a one-to-one curve for the difference-sum RSS ratio (dB) in order to determine the angle but not the distance.

For a specific angle, this study uses an estimation algorithm for positioning by aggregating the results of distributed DoA modules. The algorithm is used to locate the DUT in a region of 100 m $\times$ 100 m with the DoA modules placed at the four corners. Two orientation arrangements are compared and the results show that best positioning is achieved by aligning the DoA modules to the center of the region. The average positioning error for the entire region is 2 m, which is about 2% of the size of the region.

The angular error is large if the angle of incoming source is large, but accuracy is increased by using a pseudo inverse solution. The DoA module uses RSS only so it cannot differentiate between the right or left sides of the central direction so this study uses a minimum residual sum to resolve the angular ambiguity. A pseudo Monte Carlo method is also proposed to accelerate the simulation process and calculate the confidence range for the estimated position.

Compared to methods that use high-directivity stereo antennas for the DoA, the module proposed by this study needs not resort to dedicate circuit topology for phase measurement. It is simple and low cost, involves low power consumption, and is small size. The results show that it can achieve an angular error of less than 4% for 90% of the FoV. Using appropriate orientation, four distributed DoA modules achieve positioning with an average error of 2% in a region of 100 m $\times$ 100 m.

In this study, the DoA modules are located co-planarly, so only the projected position of DUT on this plane can be obtained. In certain applications, *e.g.*, to locate the mountaineer climbers or the elderly missing persons in the playground, the two-dimensional positioning is enough. If the three-dimensional positioning is required, there will be at least two more DoA modules facing up in the latitude direction in the region to achieve that goal.

For the context of SaR scenario, it is not easy to do the real measurement in the mountain area. The experiment conducted in the university campus is in LOS and no shade in the middle. It still demonstrates the capability of locating the DUT position without resorting to GPS through the phase-less measurement. In real SaR applications, the DUT position will correspond to the last reflection in the multipath, which is usually not far from the climbers. Since the method is phase-less, we need only one drone with a DoA module. The results of the multiple receivers can be obtained from the hovering drone. Since the drone is higher than DUT, the present algorithm yields only the projected DUT position into the plane formed by the receivers. Given the longitude and latitude, the DUT position is available from the map and the present method is still applicable.

REFERENCES

[1] M. Vossiek, L. Wiebking, P. Gulden, J. Wieghardt, C. Hoffmann, and P. Heide, "Wireless local positioning," *IEEE Microw. Mag.*, vol. 4, no. 4, pp. 77–86, Dec. 2003.

[2] T.-P. Chou, T.-Y. Lin, and C.-C. Li, "The mountaineer's rescue system in Taiwan," in *Proc. Int. Carnahan Conf. Secur. Technol.*, 1989, pp. 247–250.

[3] K. Ishisaka, K. Kobayashi, Y. Oguri, and Y. Honma, "Development of climber location information sharing system in Japanese northern Alps," in *Proc. URSI AP-RASC*, New Delhi, India, Mar. 2019, p. 1.

[4] A. Calabro and R. Giuliano, "Integrated Wi-Fi and LoRa network on UAVs for localizing people during SAR operations," in *Proc. AEIT Int. Conf. Electr. Electron. Technol. Automot. (AEIT AUTOMOTIVE)*, Nov. 2021, pp. 1–6.

[5] P. Georgopoulos, B. McCarthy, and C. Edwards, "Location awareness rescue system: Support for mountain rescue teams," in *Proc. 9th IEEE Int. Symp. Netw. Comput. Appl.*, Jul. 2010, pp. 243–246.

[6] S. Sambolek and M. Ivasic-Kos, "Automatic person detection in search and rescue operations using deep CNN detectors," *IEEE Access*, vol. 9, pp. 37905-37922, 2021.

[7] G. M. Bianco, R. Giuliano, G. Marrocco, F. Mazzenga, and A. Mejia-Aguilar, "LoRa system for search and rescue: Path-loss models and procedures in mountain scenarios," *IEEE Internet Things J.*, vol. 8, no. 3, pp. 1985–1999, Feb. 2021.

[8] J. A. Besada, I. Campana, L. Bergesio, A. M. Bernardos, and G. de Miguel, "Drone flight planning for safe urban operations: UTM requirements and tools," in *Proc. IEEE Int. Conf. Pervasive Comput. Commun. Workshops (PerCom Workshops)*, Kyoto, Japan, Mar. 2019, pp. 924–930.

[9] S. Young and K. Holton. (Dec. 20, 2018). Drones paralyze British airport, grounding Christmas travellers. Aerospace and Defence. [Online]. Available: https://www.reuters.com/article/us-britain-drones-gatwick-idUSKCN1OI2TN

[10] J. Duplouy, C. Morlaas, H. Aubert, P. Potier, P. Pouliguen, and C. Djoma, "Wideband and reconfigurable vector antenna using radiation pattern diversity for 3-D direction-of-arrival estimation," *IEEE Trans. Antennas Propag.*, vol. 67, no. 6, pp. 3586–3596, Jun. 2019.

[11] A. H. Muqaibel, S. A. Alawsh, A. I. Oweis, and M. S. Sharawi, "Sparse DOA estimation for directional antenna arrays: An experimental validation," *IEEE Sensors J.*, vol. 21, no. 4, pp. 5173–5184, Feb. 2021.

[12] M. Burtowy, M. Rzymowski, and L. Kulas, "Low-profile ESPAR antenna for RSS-based DoA estimation in IoT applications," *IEEE Access*, vol. 7, pp. 17403–17411, 2019.

[13] M. Hartmann, T. Nowak, J. Robert, H.-M. Troger, A. Heuberger, and J. Thielecke, "A low-cost RSSI based localization system design for wildlife tracking," in *Proc. Radio Antenna Days Indian Ocean (RADIO)*, Belle Mare, Mauritius, Sep. 2015, pp. 1–2.
[14] S. He and S.-H. G. Chan, "Wi-Fi fingerprint-based indoor positioning: Recent advances and comparisons," *IEEE Commun. Surveys Tuts.*, vol. 18, no. 1, pp. 466–490, 1st Quart., 2015.
[15] P. Bahl and V. N. Padmanabhan, "RADAR: An in-building RF-based user location and tracking system," in *Proc. INFOCOM*, vol. 2, 2000, pp. 775–784.
[16] C. Chen, Y. Chen, Y. Han, H.-Q. Lai, and K. J. R. Liu, "Achieving centimeter-accuracy indoor localization on WiFi platforms: A frequency hopping approach," *IEEE Internet Things J.*, vol. 4, no. 1, pp. 111–121, Feb. 2017.
[17] C. Chen, Y. Chen, Y. Han, H.-Q. Lai, F. Zhang, and K. J. R. Liu, "Achieving centimeter-accuracy indoor localization on WiFi platforms: A multi-antenna approach," *IEEE Internet Things J.*, vol. 4, no. 1, pp. 122–134, Feb. 2017.
[18] J. L. Gómez-Tornero, D. Cänete-Rebenaque, J. A. López-Pastor, and A. S. Martínez-Sala, "Hybrid analog-digital processing system for amplitude-monopulse RSSI-based MIMO WiFi direction-of-arrival estimation," *IEEE J. Sel. Topics Signal Process.*, vol. 12, no. 3, pp. 529–540, Jun. 2018.
[19] J. Werner, J. Wang, A. Hakkarainen, D. Cabric, and M. Valkama, "Performance and Cramer–Rao bounds for DoA/RSS estimation and transmitter localization using sectorized antennas," *IEEE Trans. Veh. Technol.*, vol. 65, no. 5, pp. 3255–3270, May 2016.
[20] F. Dressler, S. Ripperger, M. Hierold, T. Nowak, C. Eibel, B. Cassens, F. Mayer, K. Meyer-Wegener, and A. Kolpin, "From radio telemetry to ultra-low-power sensor networks: Tracking bats in the wild," *IEEE Commun. Mag.*, vol. 54, no. 1, pp. 129–135, Jan. 2016.
[21] T. Nowak, M. Hartmann, T. Lindner, and J. Thielecke, "Optimal network topology for a locating system using RSSI-based direction finding," in *Proc. Int. Conf. Indoor Positioning Indoor Navigat. (IPIN)*, Banff, AB, Canada, Oct. 2015, pp. 1–5.
[22] T. Nowak, M. Hartmann, L. Patino-Studencki, and J. Thielecke, "Fundamental limits in RSSI-based direction-of-arrival estimation," in *Proc. 13th Workshop Position., Navigat. Commun. (WPNC)*, Bremen, Germany, 2016, pp. 1–6.
[23] D. M. Pozar, *Microwave Engineering*. Hoboken, NJ : Wiley, 2012. ch. 7, sec. 8.
[24] G. M. Dimitris, K I. Vinay, and M K. Stephen, *Statistical and Adaptive Signal Processing: Spectral Estimation Signal Modeling Adaptive Filtering and Array Processing*, vol. 46. Norwood, MA, USA: Artech House, 2005, pp. 411–420.
[25] S. Chakrabarty and E. A. P. Habets, "A Bayesian approach to informed spatial filtering with robustness against DOA estimation errors," *IEEE/ACM Trans. Audio, Speech, Language Process.*, vol. 26, no. 1, pp. 145–160, Jan. 2018.

SHIH-YI HUANG was born in Kaohsiung, Taiwan. He received the B.S. degree in electrical engineering from Fujen Catholic University and the M.S. degree from the Graduate Institute of Communication Engineering, National Taiwan University, Taipei, Taiwan, in 2017 and 2021, respectively. His research interests include AIoT, drones positioning, and antennas.

RUEY-BEEI WU was born in Tainan, Taiwan. He received the B.S.E.E. and Ph.D. degrees from the National Taiwan University, Taipei, in 1979 and 1985, respectively. He joined as a Faculty Member of the Department of Electrical Engineering, National Taiwan University, in 1982, where he is currently a Professor, and he worked as the chairperson, from 2004 to 2007. He has been with the Graduate Institute of Communications Engineering, since 1997. He was a Post Doctor at IBM, in 1986, and was a Visiting Professor at UCLA, in 1994, and Gent University, in 2009. He was appointed as the Director of the National Center for High-Performance Computing, from 1998 to 2000, and worked as the Director General of the Planning and Evaluation Department, from 2002 to 2004, both under the National Science Council (NSC). He also served as the President of the Institute for Information Industry (III), from 2012 to 2016. His research interests include computational electromagnetics, transmission line and waveguide discontinuities, microwave and millimeter wave passive components, and electromagnetic design for advanced packaging and systems. He served as the Chair of the IEEE Taipei Section, from 2007 to 2009, and received the R10 Outstanding Volunteer Award, the R10 Distinguished Large Section Award, the MGA Outstanding Large Section Award, and the Innovation Award, in 2009. He received the NSC Distinguished Research Awards, in 1990, 1993, 1995, and 1997, and was given the Outstanding Electrical Engineering Professor Award by the Chinese Institute of Electrical Engineers, in 1999. He received the Best Paper Award from IEEE TRANSACTIONS ON ADVANCED PACKAGING, in 2009, the Outstanding Research Award from the Pan Wen Yuan Foundation, in 2013, and the Academic Award from the Ministry of Education, in 2013. He served as an Associate Editor of the IEEE TRANSACTIONS ON MICROWAVE THEORY AND TECHNIQUE, from 2005 to 2008, and the IEEE TRANSACTIONS ON ADVANCED PACKAGING, from 2009 to 2012.